Recent advances in crystal optics/Avancées récentes en optique cristalline

Ceramic YAG lasers

Takunori Taira

Laser Research Center for Molecular Science, Institute for Molecular Science (IMS), 38 Nishigonaka, Myodaiji, Okazaki 444-8585, Japan

Available online 13 October 2006

Invited Paper

Abstract

Transparent polycrystalline that is 'ceramic' laser materials offer numerous advantages over melt growth methods, including faster production times, their solid solution allows the fabrication of multi-phase transition materials that are highly homogeneous and they show the ability to engineer profiles and structures before sintering. Much progress has been made in improving the optical quality of ceramics, as well as exploring new laser materials. Successfully developed concentrated Nd:YAG ceramics has opened the way for drastic heat reduction by pumping directly into the upper laser level. Especially for the composite structure fabrication, it is attractive because of low fabrication costs by mass production and short delivery times compared with conventional diffusion bonding. In this research, we report on >300 W continuous wave (CW) laser operation in an edge-pumped 300 μm-thick, single crystal Yb:YAG/ceramic YAG composite microchip. ***To cite this article: T. Taira, C. R. Physique 8 (2007).***
© 2006 Académie des sciences. Published by Elsevier Masson SAS. All rights reserved.

Résumé

Les lasers à céramiques YAG. Les matériaux lasers polycristallins transparents, ou « céramiques », offrent de nombreux avantages sur ceux élaborés par fusion, notamment des temps de production plus courts, l'accès à des solutions solides permettant la fabrication de matériaux à transition de phase multiple, une très grande homogénéité et la possibilité de définir des profils et des structures avant frittage. La qualité optique des céramiques a beaucoup progressé et de nouveaux matériaux ont été explorés. Le développement des céramiques concentrées Nd :YAG a ouvert la voie à une réduction drastique de la production de chaleur grâce au pompage direct sur le niveau supérieur. Ceci est particulièrement intéressant pour la fabrication de structures composites du fait de faibles coûts de fabrication liés à la production de masse et de délais de production courts, en comparaison du soudage par diffusion conventionnel. Ce travail décrit un laser émettant plus de 300 W en continu, basé sur une micropuce composite monocristal Yb :YAG/céramique YAG pompée par le côté. Nous discutons aussi des développements futurs, en particulier l'adaptation du profil spectral. ***Pour citer cet article : T. Taira, C. R. Physique 8 (2007).***
© 2006 Académie des sciences. Published by Elsevier Masson SAS. All rights reserved.

Keywords: Nd:YAG ceramics; CW laser; Yb:YAG/ceramic YAG

Mots-clés : Céramique Nd :YAG ; Laser continu ; Yb :YAG/céramique YAG

1. Introduction

During the last decade, numerous laser materials have been investigated to realize high efficiency and brightness output with the development of diode-pumped solid-state lasers (DPSSLs) [1]. In the 1990s, trivalent rear-earth (RE^{3+}) ion doped vanadate or apatite, instead of $Y_3Al_5O_{12}$ (YAG), were developed for highly efficient miniature lasers due to their large absorption and emission cross-sections [2,3]. However, the difficulty in growing large size crystals and their poor thermo-mechanical properties are preventing their further progress, especially for the power scaling. Recently, attention has been directed to the RE^{3+} ion-doped YAG ceramic laser material because of its numerous advantages over melt growth methods, including faster production times, its solid solution allowing the fabrication of multi-phase transition materials that are highly homogeneous, or the ability to engineer profiles and structures before sintering. Much progress has been made in improving the optical quality from ceramics, as well as exploring new laser materials.

After the first Nd:YAG ceramic laser report by A. Ikesue et al. [4], the material properties for high brightness miniature lasers were investigated [5,6]. Subsequently, T. Yanagisawa et al. have been demonstrated the Nd:YAG ceramic laser oscillation by another sintering method [7]. In this article, after the introduction of the basic properties of the transparent Nd:YAG ceramic material, we would like to discuss the next direction of advanced YAG ceramic lasers toward high brightness and an integrated compact system.

2. Basic properties of Nd:YAG ceramics

2.1. Spectroscopic properties

The energy level diagram of Nd:YAG, which is by far the most commonly used type of solid-state laser, is shown in Fig. 1 and optical properties of Nd-lasers are summarized in Table 1 [8–18]. Nd^{3+}-ion has three typical groups of transitions centered at the transitions $^4F_{3/2} \rightarrow {}^4I_{9/2}$ (~0.95 µm), $^4F_{3/2} \rightarrow {}^4I_{11/2}$ (1.06 µm), and $^4F_{3/2} \rightarrow {}^4I_{13/2}$ (~1.34 µm) for laser emission. On the other hand, the $^4I_{9/2} \rightarrow {}^4F_{5/2}$ transition (~0.81 µm) is used for DPSSLs. YVO_4 crystal belongs to the zircon ($ZrSiO_4$) tetragonal space group, and the Nd-ion in this host has, generally, similar absorption and emission spectra. Additionally, the absorption spectrum is stronger, which makes the material more suitable for diode-laser pumped microchip lasers than Nd:YAG as a low-threshold laser material at 1.064 and 1.34 µm [2,19,20]. However, its poor thermo-mechanical property is not suitable for power scaling [21]. The YAG host is a cubic crystal with space group Ia3d. It has enough high mechanical strength, good chemical stability, and high thermal conductivity to sustain the power laser operation. For the efficient operation, highly Nd doping should be required to compensate its small cross-section and low segregation coefficient in the single crystal growth.
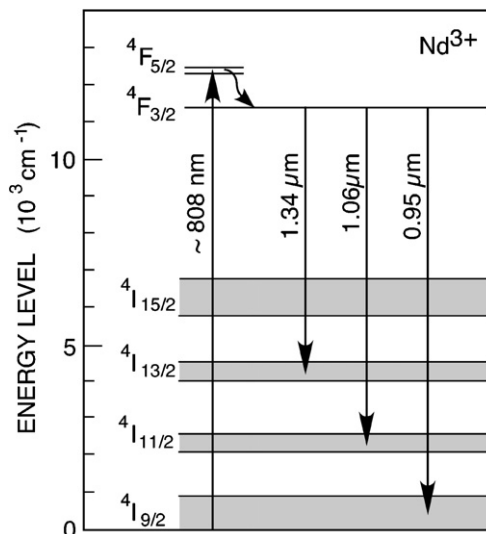

Fig. 1. The energy level diagram of Nd:YAG.

Table 1
The optical properties of Nd-lasers [8–18]

Material	Concentration C_{Nd}	Emission					Absorption		
		Wavelength λ_e (μm)	Cross-section σ_e (10^{-19} cm^2)	Lifetime τ_f (μs)	$\sigma_e \tau_f$ (a.u.)	Spectrum width $\Delta\lambda_e$ (nm)	Wavelength λ_p (nm)	Abs. Coefficient α_a (cm^{-1})	Spectrum width $\Delta\lambda_a$ (nm)
Nd:YAG	1.0 at%	0.946	0.24	225	0.09	0.7	808.4	9.1	1.2
[Y$_3$Al$_5$O$_{12}$]		1.0642	2.63		1.00	1.1	868.6	2.8	1.1
		1.319/1.338	0.37/0.21		0.14/0.08	1.2/1.2	885.4	1.6	2.8
Nd:YVO	1.0 at%	0.914	0.31	84.1	0.04	3.2	808.7	53.5*	1.7
[Nd:YVO$_4$]		1.0641	14.1		2.00	1.1	879.8	39.8	1.4
		1.342	1.35		0.19	2.0			
Nd:GVO	~1.0 at%	0.912	0.24	83.4	0.03	3.2	808.2	33.2*	1.5
[Nd:GdVO$_4$]		1.0628	10.3		1.45	1.0	879.0	24.6	1.4
		1.341	1.38		0.19	1.9			
Nd:GGG	1.7 at%	0.933/0.937	0.27/0.23	200	0.09/0.08	0.8/0.8	807.6	14.5	1.1
[Nd:Gd$_3$Ga$_5$O$_{12}$]		1.062	1.54		0.52	0.90	871.0	5.9	1.5
		1.323/1.331	0.34/0.34		0.11	1.4/1.4			
Nd:SVAP	1.0 at%	1.0654	5.00	210	1.77	1.6	809.0	16.9	1.6
[Sr$_5$(VO$_4$)$_3$F]		1.33	2.10		0.75				
Nd:FAP		1.0629	5.00	230	1.94	0.6	807.0		1.6
[(PO$_4$)$_3$F]						[1.62×10^{-19} cm^2]			
Nd:SFAP	0.72 at%	1.0585	5.40	298	2.72	0.6	805.2	27.4	1.6
[Sr$_5$(PO$_4$)$_3$F]		1.328	2.30		1.16				
Nd:YLF	1.0 at%	1.047	1.87	460	1.45	1.37	792.0	7.0	2.0
[YLiF$_4$]		1.053	1.25		0.97			2.4	1.8
Nd:glass	5.0 at%	1.054	0.40	315	0.21	20	800.0	3.00	13
NPP	0.40×10^{20} cm^{-3}	1.0512	2.00	115	0.22	5.1	800		
[NdP$_5$O$_{14}$]									
LNP	0.43×10^{20} cm^{-3}	1.047	3.20	135	0.41		800	40.0	
[LiNdP$_4$O$_{12}$]		1.320	0.38		0.05				
NYAB	1.95×10^{20} cm^{-3}	1.062	4.46	56	0.24		808	8.30	8.4
[Nd:YAl$_3$(BO$_3$)$_4$]									
Nd:LSB	5.1×10^{20} cm^{-3}	1.062	1.30	118	0.14	4	808	36.0	3.0
[Nd:LaSc$_3$(BO$_3$)$_4$]									

* Note: $\alpha_a = 65$ cm^{-1} at 808 nm for 1 at% Nd:GdVO$_4$, $\alpha_a = 40$ cm^{-1} at 808 nm for 1 at% Nd:YVO$_4$ in Ref. [8].
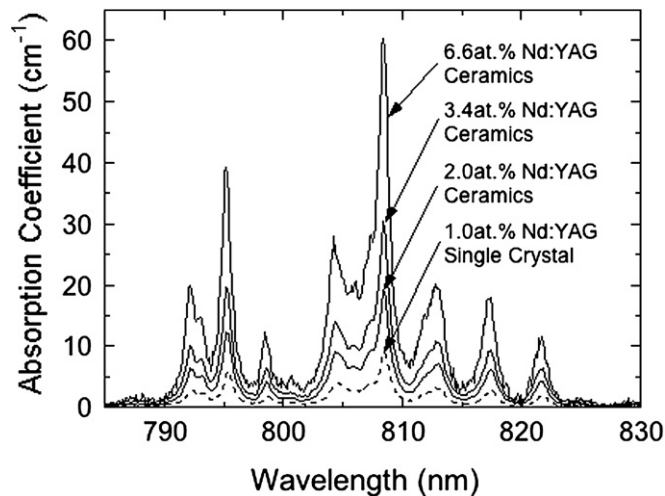

Fig. 2. Absorption spectra of Nd:YAG ceramics (solid curves) and Nd:YAG single crystal (dashed curve) [22].
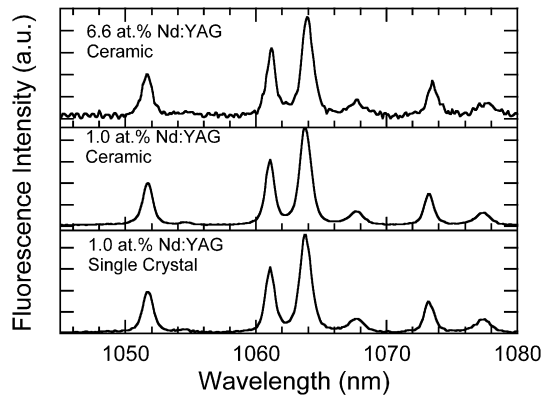
Fig. 3. The emission spectra of Nd:YAG ceramics and the single crystal [23].

Fig. 2 shows the absorption spectra of the 2.0, 3.4, and 6.6 at% Nd:YAG ceramics, which were fabricated by A. Ikesue, and the 1.0 at%-doped single crystal (Scientific Material Co.) [22]. The measurements at room temperature were carried out using a spectrophotometer at a 0.2 nm resolution. The spectrum of the 1.0 at%-doped ceramic, which is not shown in Fig. 2, was nearly identical to that of the single crystal. The absorption increases in proportion to the Nd^{3+} concentration C_{Nd}. At the peak absorption wavelength of 808 nm, the 3.4 at% Nd:YAG ceramic has an absorption coefficient of 30.4 cm^{-1}, which is large enough for micro-lasers. The absorption spectrum of the 8.2 at%-doped ceramic is not shown in Fig. 2 because its absorbance was too large to accurately obtain the absorption coefficients around the peak absorption wavelength of 808 nm, but the absorption coefficients at the other measured wavelengths were eight times larger than that of the 1.0 at%-doped single crystal. The emission spectra of 1.0 and 6.6 at% Nd:YAG ceramics are same as that of 1.0 at% Nd:YAG single crystal, as shown in Fig. 3 [23].

2.2. Thermal properties

From the point of view of a power scaling, solid-state laser medium should have (i) highly thermal conductivity, κ, and tensile strength, (ii) the ability of highly quality large size material growth, and (iii) highly transparency around oscillation and pumping wavelength. As a figure of merit for thermo-mechanical property, the thermal shock parameter, R_T, of materials is discussed [24]. Thermally induced rupture or catastrophic failure of a crystal is then the primary limiting factor to the attainment of higher average powers in the solid-state laser material. In the typical side pumped rod-type lasers, the maximum extractable power P_{ex} available is

$$P_{ex} \leqslant \frac{8\pi R_T L}{\chi} \tag{1}$$

where L is the rod length, and χ is the heating parameter defined as heat deposited per unit stored energy [25]. From Eq. (1), it is clear that the maximum extractable power is directly proportional to the thermal shock parameter, which is roughly proportional to κ/α^2 (α is the thermal expansion coefficient). The main interest of heavy doped Nd:YAG ceramics, which have a strong absorption coefficient even if compared with Nd:YVO$_4$, is the thermal conductivity for high power application. Fig. 4 shows the thermal conductivities of Nd:YAG ceramics as a function of C_{Nd} at 20 °C by the laser flash method [5]. They are as high as that of single-crystal YAG even at high Nd concentrations, 9.0 W/mK for 6.6 at% doped YAG ceramics. Although Nd:YVO$_4$ is a popular material for microchip lasers because its absorption coefficient at the pump wavelength is high, realizing a high power microchip laser is difficult since its thermal conductivity seems to be as low as half that of YAG [21]. On the other hand, in spite of its good thermo-mechanical properties, Nd:YAG single crystals are not suitable for highly efficient microchip lasers [26] due to their small absorption coefficients, since high-quality YAG crystals with Nd doping beyond 1.5 at% are hardly obtainable by the standard Czochralski method. However, Nd:YAG ceramics have both the advantages of Nd:YVO$_4$ and Nd:YAG single crystals [5].
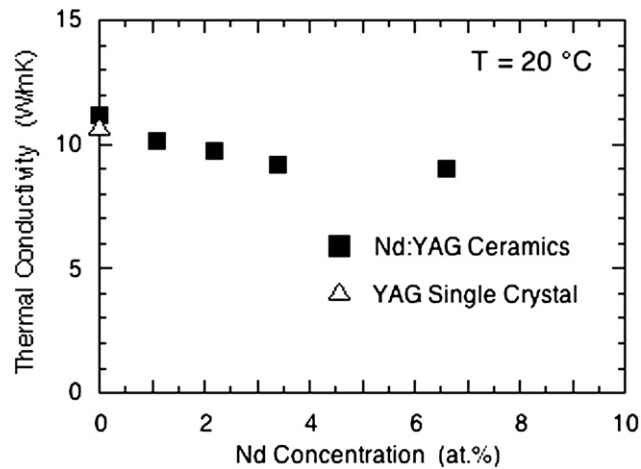
Fig. 4. The thermal conductivities of Nd:YAG ceramics as a function of Nd concentration [5].
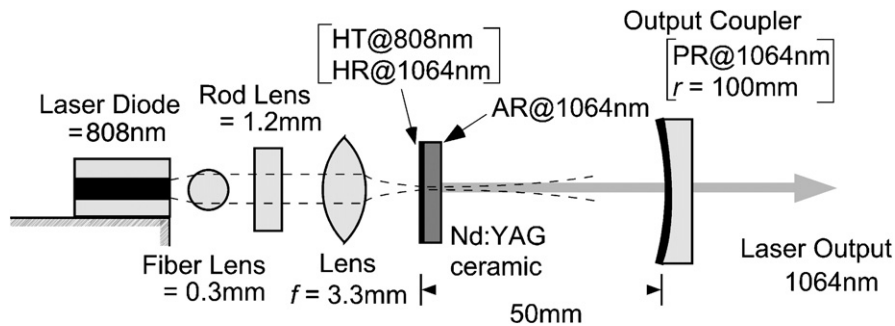

Fig. 5. Schematic of the diode-pumped laser oscillation [22].

2.3. Diode pumped microchip lasers

Fig. 5 shows the schematic of the laser setup. We used a diode laser oscillating at 808 nm as a pump source. The pump beam was collimated with a fiber and a rod lens and focused onto the samples. The sample thicknesses were less than 1 mm, and a nearly circular pump beam shape, ∼90 μm radius, was realized in the medium. The input facet of the sample was high transmission and high-reflection (HR) coated at 808 and 1064 nm, respectively, and the output facet was antireflection (AR) coated at 1064 nm. An output coupler with a curvature of 100 mm was used, and the cavity length was set to be 50 mm. We have observed laser oscillation in ceramic samples with up to the 3.4 at% doping [22]. Fig. 6 shows the input–output power relationships of the 2.3 and 3.4 at%-doped ceramics and the 0.9 at%-doped single crystal when an output coupler with transmittance of 4.4% was used. For the 3.4 at%-doped ceramic, 2.3 times higher output was achieved than for the single crystal, which indicates the advantages of Nd:YAG ceramics as highly efficient miniature or microchip lasers [22].

Next, we have evaluated the cavity losses by obtaining the slope efficiencies η'_ss, which were determined from the relation between the absorbed pump and the laser output power by changing the transmittance of the output coupler. Then, it was found that the loss of the 2.3 at%-doped ceramic is as low as that of the single crystal. However, the 3.4 at%-doped ceramic has much higher loss coefficient. It is presumably because the scattering loss at the grain boundaries becomes significant, since the ceramics with higher neodymium concentration have smaller grain sizes, i.e., an increased number of the grain boundaries. The slope efficiency of the ceramics was found to be higher than that of the single crystal. That is because the mode-matching efficiencies of the ceramics are higher than that of the single crystal; owing to their larger absorption coefficients; the absorption depths in the ceramics are shorter, resulting in larger mode overlap between the pump and the laser beams in the sample [22]. This concentrated Nd:YAG ceramics has enough gain to realize the intracavity frequency doubled system with KTP crystal, as shown in Fig. 7 [27].
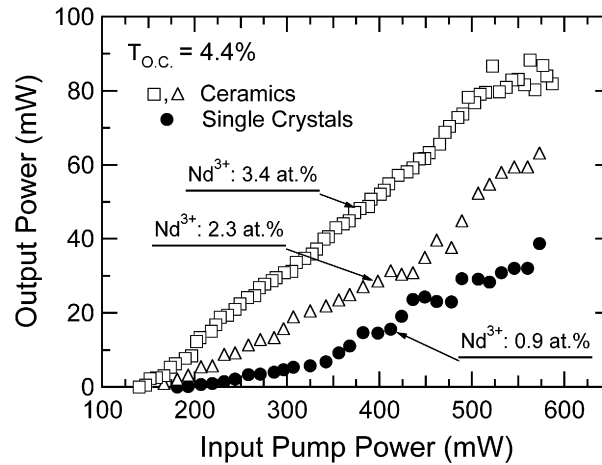
Fig. 6. Dependence of the output power on the input pump power for the 3.4 and 2.3 at% Nd:YAG ceramics and the 0.9 at% Nd:YAG single. Thicknesses of the 3.4, 2.3, and 0.9 at%-doped samples were 847, 868, and 719 mm, respectively [22].
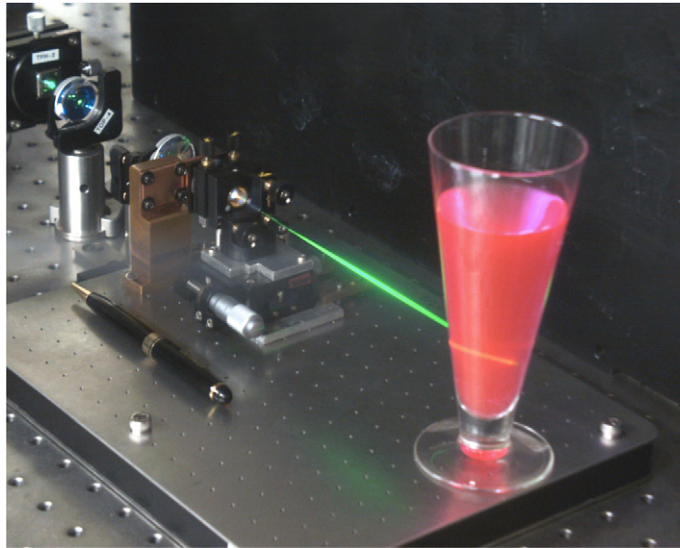

Fig. 7. Intracavity frequency doubled Nd:YAG ceramic laser with KTP [27].

Recently, we have succeeded in obtaining the laser oscillation even with uncoated 6.8 at% doped Nd:YAG ceramics, by the Ti:sapphire laser pumping [28].

2.4. Thermally induced birefringence

The thermal problem is an important issue for the power scaling of solid-state lasers. In order to understand the thermal behavior of ceramics, we have investigated the thermal-birefringence-induced depolarization effect in Nd:YAG ceramics, which should be an essential issue in controlling polarization under high-power operation. The thermal birefringence effect was measured with the pump–probe experiment as shown in Fig. 8 [29]. A Ti:sapphire laser oscillating at 808 nm was used as the pump source with the maximum input power of 3 W. The pump beam was focused onto the sample with a radius of 80 μm. A linearly polarized (in the y direction) He–Ne laser beam of 1-mm radius was used as the probe. After it passed through the sample, the probe beam was reflected at the plane surface of the focusing lens and went back through the sample again. Part of the beam was reflected at the beam splitter, and only the depolarized (i.e., x-polarized) component of the probe beam transmitted the analyzer, which was in the
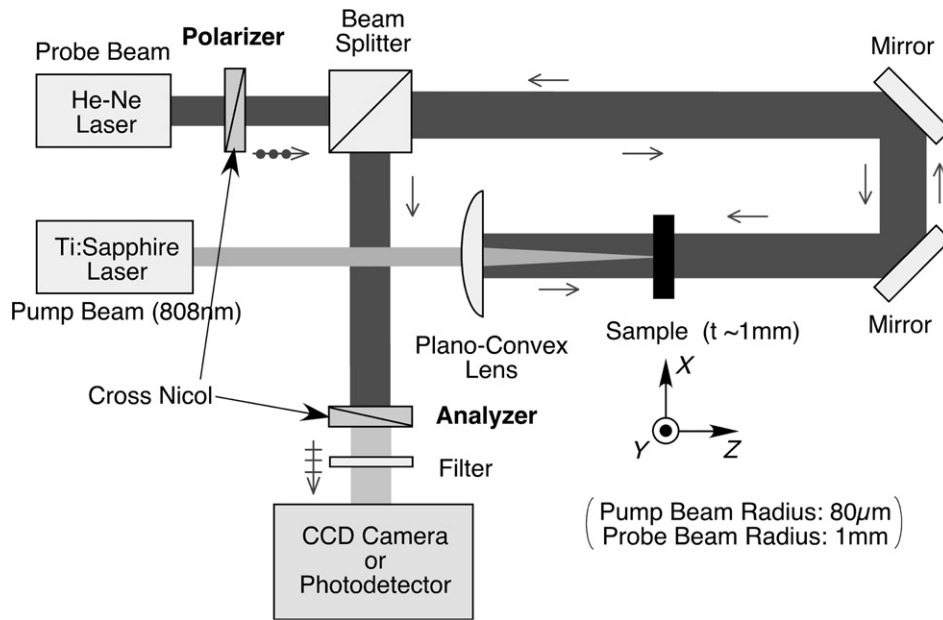
Fig. 8. Experimental setup for measurement of the thermally induced birefringence depolarization in the laser material [29].
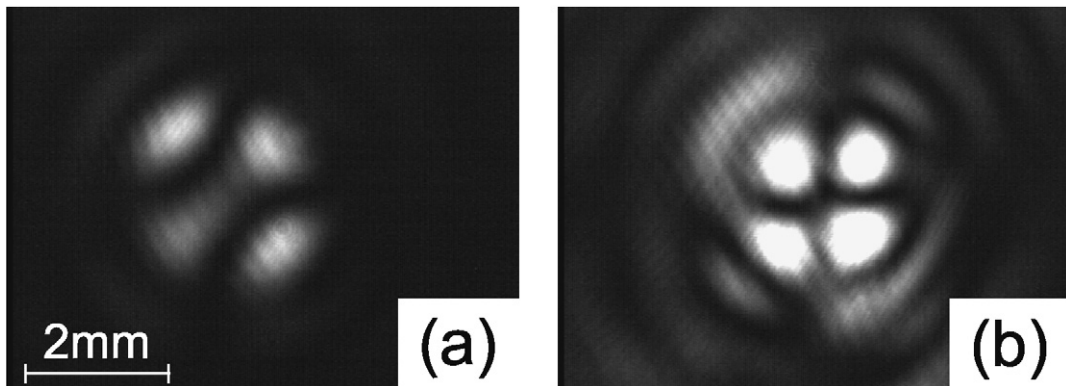

Fig. 9. Depolarized beam patterns for a (a) 1.0 at% Nd:YAG single crystal ((111)-cut sample) and (b) 3.4 at% Nd:YAG ceramic at the absorbed pump power of 1052 and 1085 mW, respectively [29].

cross-nicol configuration with the polarizer. The depolarized beam passed through a filter that absorbed the pump beam, and its pattern was observed with a CCD camera. The beam's power was measured with a photodetector. The measured samples were 1.0-, 1.3-, 2.0-, and 3.4-at% Nd^{3+}-doped YAG ceramics and 1.0-and 1.3-at% Nd:YAG single crystals. The thickness of each sample, L, was 1 mm, and (111)-cut samples were used. Fig. 9 shows the depolarized beam patterns of the 1.0-at% Nd:YAG single crystal and the 3.4-at% Nd:YAG ceramic at absorbed pump powers of 1052 and 1085 mW, respectively. Since the thermal birefringence in the (111) plane of a Nd:YAG single crystal occurs between the radial and the azimuthal directions, the depolarized beam that passes through the analyzer forms a four-leaf-like pattern, shown in Fig. 9(a). Although the same pattern was observed for the ceramics, the depolarization was enhanced compared with that of the single crystal (Fig. 9(b)). The depolarization is defined as the ratio of the depolarized power to the total probe power, $D_{\mathrm{pol}} = P_\perp/(P_\parallel + P_\perp)$. Fig. 10 shows the depolarization as a function of Nd-concentration at the absorbed pump power of 1000 mW. We found that the depolarization is nearly the same for the ceramic and the single-crystal YAG for the same Nd-concentrations [29]. The thermal birefringence in the $\langle 111 \rangle$ direction, along which a conventional Nd:YAG rod is grown, is given by
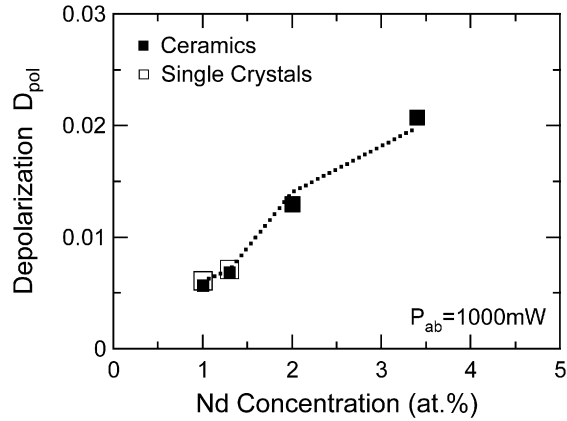
Fig. 10. Depolarization as a function of the Nd-concentration for the ceramic and single-crystal samples at the absorbed pump power of 1000 mW. The dotted line shows the calculated result with taking account of dependence of the thermal loading on the Nd-concentration [29].
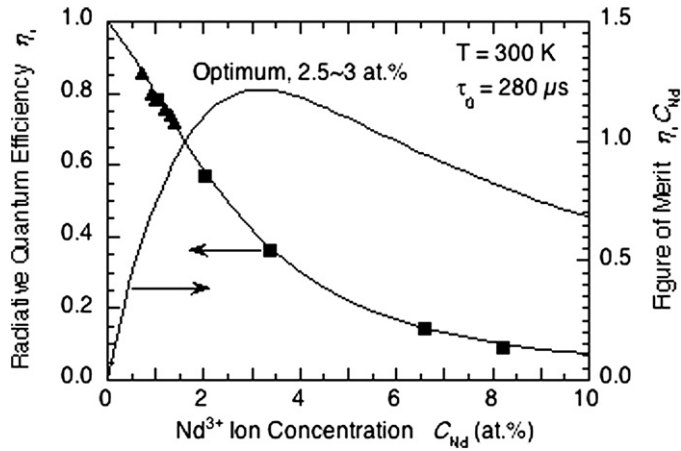

Fig. 11. The radiative quantum efficiency of Nd:YAG as function of Nd-concentration [33].

$$\Delta n(r, z) = -\frac{n_0^3}{6}(p_{11} - p_{12} + 4p_{44}) \times \left[\varepsilon_r(r, z) - \varepsilon_\phi(r, z)\right] \tag{2}$$

where ε_r and ε_ϕ are the strain tensors in the radial and the azimuthal directions in the (111) plane, respectively, n_0 is the initial refractive index, and p_{mn} are the photoelastic coefficients [30]. However, the birefringence in other directions is quite different from that in Eq. (2), and the dependence of depolarization on the rotation angle of polarization measured for (100)- and (110)-cut crystals oscillated around the constant value of depolarization for a (111)-cut crystal [31]. Because YAG ceramics consist of many YAG single-crystal grains (their sizes are several tens of micrometers) with various directions, which means that the birefringence effect in a ceramic sample is the average of the effect in those grains, we suggest our results indicate that the average is close to the birefringence effect for (111)-cut Nd:YAG single crystals.

Moreover, it was also found that the depolarization became larger in samples with higher Nd-concentrations, even if the same absorbed pump power. To understand this reason, we would like to discuss the thermal loading, which is written as, [32]:

$$\eta_h = 1 - \eta_p\left[(1 - \eta_l)\eta_r(\lambda_p/\lambda_f) + \eta_l(\lambda_p/\lambda_l)\right] \tag{3}$$

where η_p is the pump quantum efficiency ($\sim$1), η_l is the fraction of excited ions that are extracted by stimulated emission, η_r is the radiative quantum efficiency, λ_p is the pump wavelength (808 nm), λ_f is the average fluorescence wavelength (1038 nm), and λ_l is the stimulated-emission wavelength. For a highly Nd-doped sample, in which the interaction between Nd-ions is significant, the amount of non-radiative relaxation increases and radiative quantum

efficiency gets smaller. Under the condition of no laser extraction, i.e., $\eta_l = 0$, the smaller quantum efficiency causes larger thermal loading, that is, more heat generation in the sample, even at the same absorbed power, and this induces larger thermal birefringence. The solid curve in Fig. 10 shows the calculated result, for which we used the values of thermal loading obtained from the radiative quantum efficiency as shown in Fig. 11 [33,34]. The agreement between experiment and rough estimation is satisfactory. When lasing occurs, however, thermal birefringence is expected to be greatly reduced because η_l is then 1, so the thermal loading is independent of radiative quantum efficiency. This means that cw or high-repetition-rate, high-average-power Q-switched operation is preferable for highly Nd-doped ceramics.

3. Advanced ceramic lasers

3.1. Directly pumping to laser upper level in concentrated Nd:YAG ceramics

The quantum defect between the pump and laser emission wavelengths influences the laser parameters, such as the laser emission threshold and slope efficiency and the generation of heat by non-radiative processes inside the system of active ions. Traditionally the DPSSL based on Nd use for pump the strong absorption to the level $^4F_{5/2}$ (Fig. 12(a)) although the first experiments on Nd:YAG, both in transverse or end-pumped configurations used for pump the much weaker absorption to the emitting level $^4F_{3/2}$ [33–39]. The parasitic quantum defect between the levels $^4F_{5/2}$ and $^4F_{3/2}$ is of the order of 900 cm^{-1} and it contributes to the reduction of the performances of these lasers. A recent investigation of the resonant pump in $^4F_{3/2}$ level (Fig. 12(b)) of 1-at% Nd:YAG crystals reveals [35] the favorable influence of this means of pump on the emission threshold and slope efficiency. However, owing to the weak absorption in $^4F_{3/2}$ the use of low concentrated laser materials prevents the construction of compact high power lasers. By using the concentrated Nd:YAG ceramics, a systematic improvement of the slope efficiency and oscillation threshold under the hot-band pump of the transitions $Z_2 \rightarrow R_1$ and $Z_3 \rightarrow R_2$ in $^4I_{9/2} \rightarrow {}^4F_{3/2}$ absorption (Fig. 12(c)) is expected from the reduction of the pump quantum defect compared with the conventional 808-nm pumping. The increase of the threshold due to concentration quenching in the Nd:YAG is compensated by the increased pump absorption efficiency in the concentrated materials.
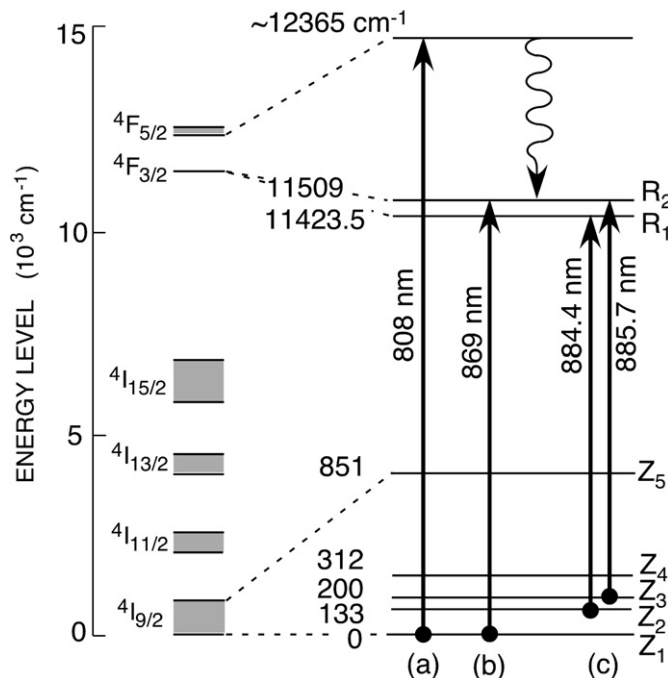

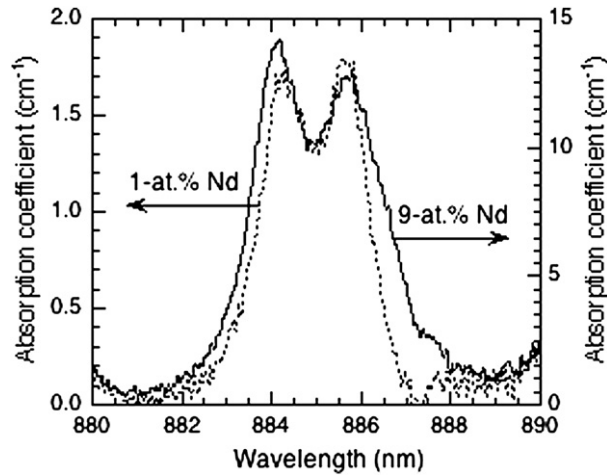Fig. 12. Energy level diagram of Nd:YAG with description of (a) conventional, (b) direct and (c) hot-band direct pump.

Fig. 13. $^4I_{9/2} \rightarrow {}^4F_{3/2}$ room temperature absorption profile of Nd:YAG ceramics of various doping levels [33].

The most intense of these lines in the room temperature $^4I_{9/2} \rightarrow {}^4F_{3/2}$ is the transition $Z_1 \rightarrow R_2$ (868.9 nm), but the reduced FWHM (<0.88 nm) makes it unsuitable for diode laser. A better prospect in this respect [33,35], is the double-peaked band centered at ~885 nm that collects the hot-band transitions $Z_2 \rightarrow R_1$ (885.7 nm) and $Z_3 \rightarrow R_2$ (884.3 nm) of the $^4I_{9/2} \rightarrow {}^4F_{3/2}$ absorption as shown in Fig. 13. The absorption coefficients of the two peaks at the room temperature are nearly equal, ~5.7 cm^{-1} for 3.5-at% Nd, while the dip between peaks has an absorption coefficient about 15% lower. The FWHM of this band is much larger than for other absorption bands in the $^4I_{9/2} \rightarrow {}^4F_{3/2}$ spectrum (~3 nm), making it suitable for diode laser pump. The fractional thermal population coefficients of the crystal field components Z_2 and Z_3 of the ground state at the room temperature are 0.245 and 0.178, respectively, i.e. they collect 42.3% from the total population of $^4I_{9/2}$, as compared to 46.5% in the lowest component Z_1. However, the concentrated Nd:YAG should loose its radiative quantum efficiency by the effect of migration on the emission decay such as down-conversion cross relaxation $(^4F_{3/2}, {}^4I_{9/2}) \rightarrow ({}^4I_{15/2}, {}^4I_{15/2})$. Further, this energy transfer function is used to estimate the emission quantum efficiency, η_r. As shown in Fig. 11, η_r decreases with the Nd concentration, C_{Nd}, with an unfavorable effect on the emission threshold. However, this decrease is not strong enough to annihilate the effect of the increasing pump absorption efficiency at high Nd concentrations: the product $\eta_r C_{Nd}$ that can be taken as a figure of merit for the laser potential of these materials shows values larger than for 1 at% Nd up to the region of 8 at% Nd, with the maximum around 3 at%. This indicates that the highly doped Nd:YAG components can be used for construction of efficient solid-state lasers in free-generation regime.

The spectroscopic and laser emission data [36] suggest that the pumping into the emitting level, at 885 nm, can be used for the construction of efficient microchip lasers with concentrated Nd:YAG components. Owing to a deeper penetration of the pump inside of the active component and to reduced heat generation, the pumping into the emitting level in these laser materials can be a suitable solution for construction of high-power lasers with emission into infrared or visible spectrum [37]. This concept can be easily extended to other concentrated Nd laser materials such as Nd-vanadates [38,39].

3.2. Composite structure: Yb:YAG single crystal/YAG ceramics composite laser

A trivalent-ytterbium-ion (Yb^{3+}) doped YAG has had attention as an attractive high power and high efficiency diode-pumped solid-state laser for the past few years, because it has a high quantum efficiency of over 90% (Figs. 14 and 15), reduced heat generation in the laser material and a longer upper-state lifetime of ~1 ms. Moreover, it has no undesirable loss processes such as excited-state absorption, upconversion, and concentration quenching owing to its simple electric structure. As a result, Yb:YAG has several advantages relative to Nd:YAG for diode laser pumping [40,41]. In addition, the wide emission bandwidth of the Yb^{3+}-doped material around 1 μm allows high power tunable and ultrafast lasers [42–44]. A face-cooled active mirror, for example disk-type laser configuration [45], is one of the suitable designs for Yb:YAG; it can reduce not only the thermal lens effect but also re-absorption loss, which is
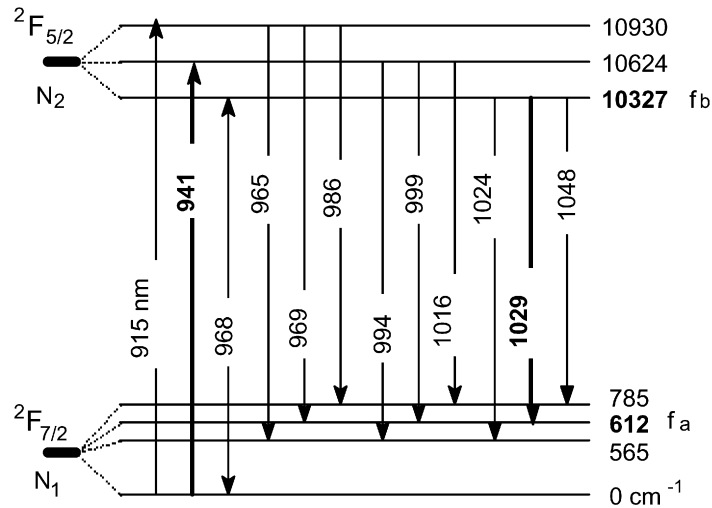
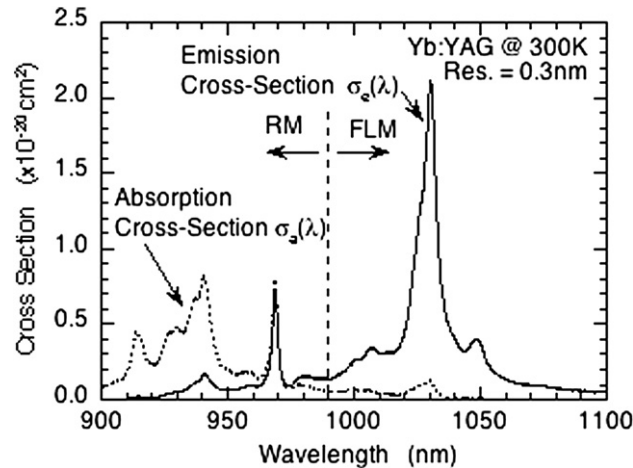Fig. 14. Energy level diagram of Yb:YAG [41].

Fig. 15. Measured absorption and emission spectrum of Yb:YAG at room temperature.

part of the nature of the quasi-four-level system, owing to the very short path length of the laser beam in the active medium. Diode edge pumping is a unique configuration for an active mirror laser, because it can avoid the complexity of a multipass-pumping optical layout [46,47]. Proper designs of the core size (diameter) and Yb concentration make efficient pump absorption possible in the core even with single-pass pumping. The first cw operation of edge-pumped Yb:YAG microchip lasers was demonstrated by using Au–Sn solder as a bond material. Up to 90 W of cw output power was obtained from a 2 mm square, 10 at% Yb:YAG core; the slope efficiency and optical-to-optical efficiency with respect to the pump power were 40% and 28%, respectively [47].

For the edge-pumped microchip lasers, the solid-solution based laser ceramics have been of great interest, because of their composite structure possibility. The fabrication process for ceramic materials is very unique and flexible, making it possible to realize new composite configurations, i.e., composite rods with a perfectly cylindrical core, which are difficult to fabricate by a conventional diffusion bonding process. In addition, the composition with ceramics is attractive for commercial use, because low fabrication costs by mass production and short delivery times are expected, due to the no seed (polycrystalline)-based fabrication process [48]. Fig. 16(a) shows a photograph of the composite core-doped Yb:YAG rod fabricated by Konoshima Chemical in Japan. The central cylindrical core 5 mm in diameter is a single-crystal 5 at% Yb:YAG, the surrounding clad 10 mm in outside diameter is ceramic undoped YAG, and the rod is 30 mm long. Colorless and pore-free structures were observed in the ceramic area. The cylindrical interface
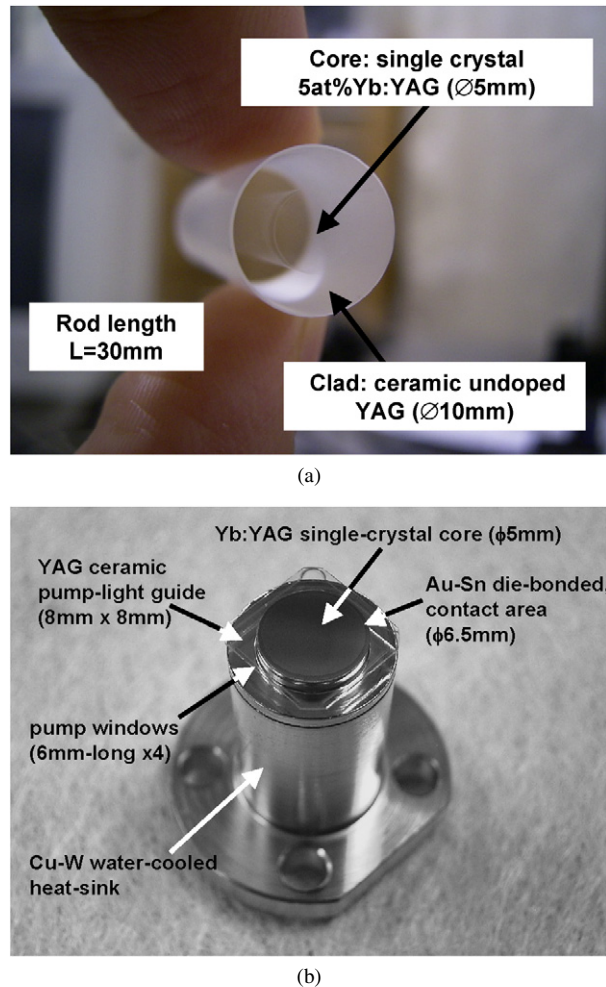
Fig. 16. (a) Photograph of hybrid composite laser rod that has single crystal Yb:YAG, cylindrical core (5 mm in diameter) surrounded by ceramic, undoped YAG clad (10 mm in diameter); (b) Hybrid composite microchip (single-crystal Yb:YAG core with ceramic YAG pump-light guide) bonded to a heat sink by a Au–Sn solder [48].

between the core and clad is less visible than conventional composite crystals made by diffusion bonding; thus, tighter and stronger binding between the two materials is expected. Microchips 300 μm thick were sliced off from the composite rod and cut to have square edges for pump windows (6 mm wide). After polishing all the surfaces, AR and HR coatings for the lasing wavelength were deposited on the two main surfaces, respectively, but no coatings were applied to the edge windows. For an active mirror cooling configuration, the HR-coated face of the chip was bonded to a water-cooled copper heat-sink by using a thermally conductive glue as seen in Fig. 16 (b). Fig. 17 shows a schematic of one of fourfold symmetrical pump systems of the directly coupled, diode edge pumped microchip Yb:YAG laser. The pump light from the diode stack consisting of 6 diodes with collimation lenses (240 W maximum output power with 940 nm operating wavelength) were focused weakly in the slow axis (SA) direction by the first spherical cylindrical lens ($f = 30$ mm) and focused tightly in the first axis (FA) direction by the second aspheric cylindrical lens ($f = 7$ mm). The focused beam spot sizes (full width at $1/e^2$ intensity) at the window edge were measured to be 4 mm and 100 mm for SA and FA directions, respectively; this means that a thin microchip 300 μm or thinner is available with a high pump coupling efficiency. The input pump light in the FA direction propagates in the ceramic YAG light-guide to the core without optical loss by total internal reflection.

Fig. 18 shows the cw output power and beam quality factor M^2 as a function of the input pump power for four different cavity configurations. In the three linear cavities the output couplers have different radii of curvature (r) of 0.25, 0.5, and 1 m with the same reflectivity of 97%. They have the same cavity length of 0.05 m. In the V-type cavity
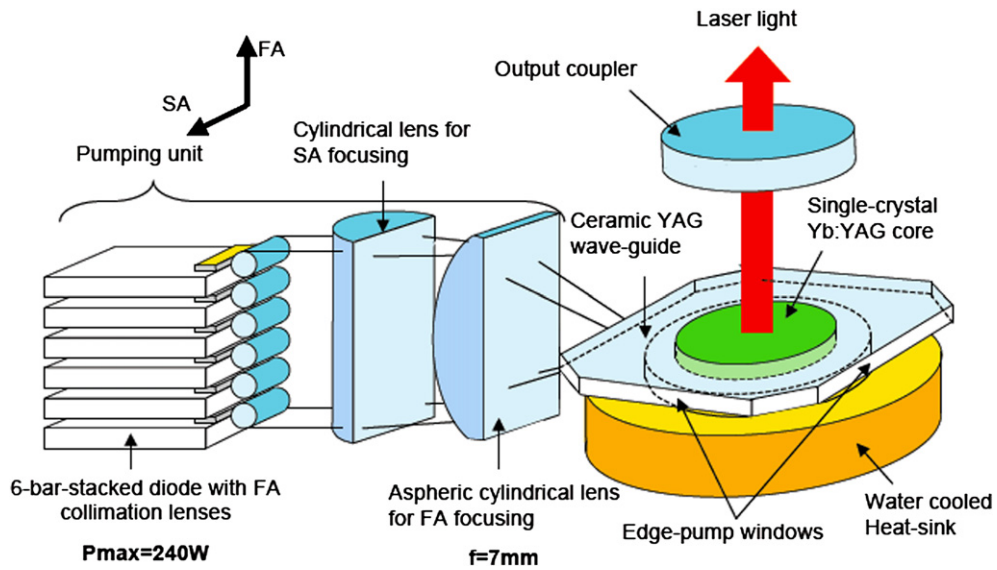
Fig. 17. Schematic of directly coupled, diode edge-pumped composite Yb:YAG microchip laser [47].
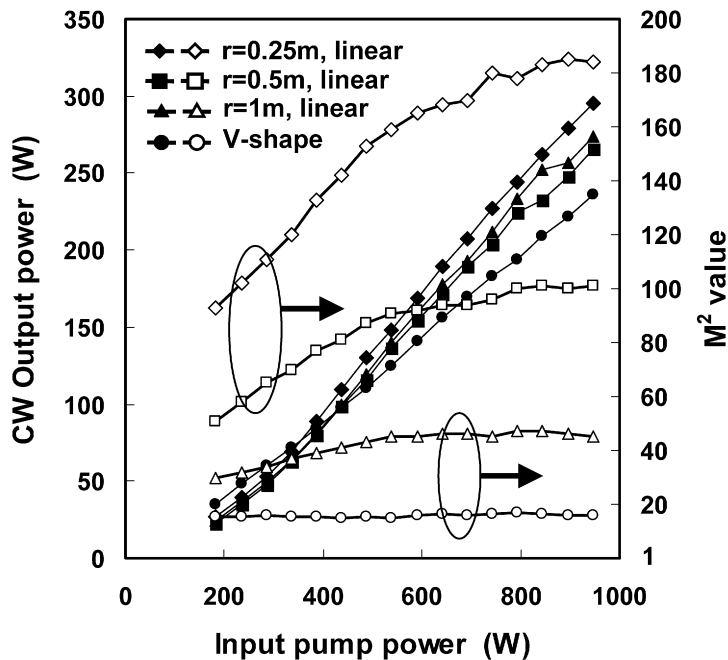

Fig. 18. Cw output power and beam quality characteristics (M^2 factor) with four different cavity configurations as a function of input pump power [47].

the output coupler has a 1 m radius of curvature with 97% reflectivity, and the other HR end mirror was flat. The length of the arm from the microchip to the end mirror was 0.3 m, and the length of the other arm to the output coupler was 0.56 m. As is seen in this figure, 340 W of cw output power (56 kW/cm^3 of output power density) was obtained at an input pump power of 946 W without a decrease in the slope efficiency in the linear cavity with the 0.25 m radius of curvature output coupler [48]. The slope and the optical conversion efficiency for the input pump power were 37% and 31%, respectively. The single-pass absorption efficiency of the pump power in the core was calculated to be 76%, taking into account the pump diode spectrum and the circular configuration of the core; thus the slope and the optical conversion efficiency for the absorbed pump power are estimated to be 49% and 41%, respectively. Although the

minimum M^2 factor of an edge pumped microchip laser was 17 as shown in Fig. 18, it simply follows the mode mismatch between the core and cavity mode. Therefore, the improved beam quality can be predicted.

4. Conclusions

In conclusion, we have reviewed the basic properties of RE^{3+}:YAG ceramics and characterized thermal properties which includes the stress induced birefringence problem. The spectroscopic properties of ceramics are the same as single crystals and confirm the advantages of heavy doping, composite structure fabrication with the new concept. By taking account of the radiative efficiency and absorption efficiency, we have discussed the potential of direct-pumping to laser upper level in Nd:YAG as an efficient high power laser. Moreover, the ability of composite device structure fabrication allows us the power scaling even if using a compact simple laser configuration. Up to 340 W CW output power (output power density of 57 kW/cm^3) was obtained in edge-pumped 300 μm-thick, single crystal Yb:YAG/ceramic YAG composite microchip. Additionally, the short pulse of 280 fs was realized in high quality Yb:YSAG disorder ceramics [49], which indicates the possibility of gain spectrum design by the sintering method. The future may herald ceramic gain media for multi-functional highly performance compact laser.

Acknowledgements

References

[1] R.L. Byer, Diode pumped solid-state lasers, Science 239 (1988) 742–747.
[2] T. Taira, A. Mukai, Y. Nozawa, T. Kobayashi, Single-mode oscillation of laser-diode-pumped Nd:YVO$_4$ microchip lasers, Opt. Lett. 16 (1991) 1955–1957.
[3] S.A. Payne, L.L. DeLoach, L.K. Smith, W.L. Kway, J.B. Tassano, W.F. Krupke, B.H.T. Chai, G. Loutts, Ytterbium-doped apatite-structure crystals: A new class of laser materials, J. Appl. Phys. 76 (1994) 497–503.
[4] A. Ikesue, T. Kinoshita, K. Kamata, K. Yoshida, Fabrication and optical properties of high performance polycrystalline Nd:YAG ceramics for solid-state lasers, J. Am. Ceram. Soc. 78 (1995) 1033–1040.
[5] T. Taira, A. Ikesue, K. Yoshida, Diode-pumped Nd:YAG ceramics lasers, OSA TOPS on Advanced Solid-State Lasers 19 (1998) 430–432.
[6] T. Taira, S. Kurimura, J. Saikawa, A. Ikesue, K. Yoshida, Highly trivalent neodymium ion doped YAG ceramic for microchip lasers, OSA TOPS on Advanced Solid-State Lasers 26 (1999) 212–215.
[7] J. Lu, J. Song, M. Prabhu, J. Xu, K. Ueda, H. Yagi, T. Yanagitani, A. Kudryashov, High-power Nd:Y$_3$Al$_5$O$_{12}$ ceramic laser, Jpn. J. Appl. Phys. 39 (2000) L1048–L1050.
[8] T. Jensen, V.G. Ostroumov, J.-P. Meyn, Spectroscopic characterization and laser performance of diode-laser-pumped Nd:GdVO$_4$, Appl. Phys. B 58 (1994) 373–379.
[9] K. Kubodera, K. Otuka, Single-transverse-mode LiNdP$_4$O$_{12}$ slab waveguide laser, J. Appl. Phys. 50 (1979) 653–659.
[10] K. Fuhrmann, N. Hodgson, F. Hollinger, H. Weber, Effective cross section of the Nd:YAG 1.0641-μm laser transition, J. Appl. Phys. 62 (1987) 4041–4044.
[11] N. Karayianis, C.A. Morrison, D.E. Wortman, Analysis of the ground term energy levels for triply ionized neodymium in yttrium orthovanadate, J. Chem. Phys. 62 (1975) 4125–4129.
[12] P.P. Yaney, L.G. DeShazer, Spectroscopic studies and analysis of the laser states of Nd^{3+} in YVO$_4$, J. Opt. Soc. Am. 66 (1976) 1405–1414.
[13] T.S. Lomheim, L.G. DeShazer, Optical-absorption intensities of trivalent neodymium in the uniaxial yttrium orthovanadate, J. Appl. Phys. 49 (1978) 5517–5522.
[14] A.W. Tucker, M. Birnbaum, C.L. Fincher, Stimulated emission cross sections of Nd:YVO$_4$ and Nd:La$_2$Be$_2$O$_5$ (BeL), J. Appl. Phys. 52 (1981) 3067–3068.
[15] D. Pruss, G. Huber, A. Beimowski, V.V. Laptev, I.A. Shcherbakov, Y.V. Zharikov, Efficient Cr^{3+} sensitized Nd^{3+}:GdScGa-garnet laser at 1.064 μm, Appl. Phys. B 28 (1982) 355–358.
[16] P. Hong, X.X. Zhang, G. Loutts, R.E. Peale, H. Weidner, M. Bass, B.H.T. Chai, S.A. Payne, L.D. DeLoach, L.K. Smith, W.F. Krupke, Lasing and spectroscopic characteristics of a new Nd laser crystal-strontium fluorovanadate, OSA Proceeding on Advanced Solid-State Lasers 20 (1994) 32–36.
[17] C. Czeranowsky, M. Schmidt, E. Heumann, G. Huber, S. Kutovoi, Y. Zavartsev, Continuous wave diode pumped intracavity doubled Nd:GdVO$_4$ laser with 840 mW output power at 456 nm, Opt. Commun. 205 (2002) 361–365.
[18] Y. Sato, T. Taira, A. Ikesue, Spectral parameters of Nd^{3+}-ion in the polycrystalline solid-solution composed of Y$_3$Al$_5$O$_{12}$ and Y$_3$Sc$_2$Al$_3$O$_{12}$, Jpn. J. Appl. Phys. 42 (2003) 5071–5074.

[19] R.A. Fields, M. Birnbum, C.L. Fincher, Highly efficient Nd:YVO$_4$ diode-laser end-pumped laser, Appl. Phys. Lett. 51 (1987) 1885–1886.

[20] G.C. Bowkett, T. Taira, G.W. Baxter, H. Teranishi, D.J. Booth, T. Kobayashi, Single-mode 1.34-μm Nd:YVO$_4$ microchip laser with cw Ti:sapphire and diode-laser pumping, Opt. Lett. 19 (1994) 957–959.

[21] Y. Kalisky, The Physics and Engineering of Solid-State Lasers, SPIE Press, Bellingham, 2006, p. 159.

[22] I. Shoji, Y. Sato, S. Kurimura, T. Taira, A. Ikesue, K. Yoshida, Optical properties and laser characteristics of highly Nd^{3+}-doped Y$_3$Al$_5$O$_{12}$ ceramics, Appl. Phys. Lett. 77 (2000) 939–941.

[23] I. Shoji, T. Taira, A. Ikesue, Ceramic lasers, IEICE Transactions C J84-C (2001) 918–925 (in Japanese).

[24] W. Koechner, Solid-State Laser Engineering, fifth ed., Springer-Verlag, Berlin, 1999, p. 412.

[25] D.C. Brown, Ultrahigh-average-power diode-pumped Nd:YAG and Yb:YAG lasers, IEEE J. Quantum Electron. QE-33 (1997) 861–873.

[26] J.J. Zayhowski, A. Mooradian, Single-frequency microchip Nd lasers, Opt. Lett. 14 (1989) 24–26.

[27] T. Taira, A. Ikesue, K. Yoshida, Performance of highly Nd^{3+}-doped YAG ceramic microchip laser, in: Conference on Lasers and Electro-Optics CLEO '99, CTuK39, 1999, pp. 136–137.

[28] V. Lupei, N. Pavel, T. Taira, Efficient laser emission in concentrated Nd laser materials under pumping into the emitting level, IEEE J. Quantum Electron. QE-38 (2002) 240–245.

[29] I. Shoji, Y. Sato, S. Kurimura, V. Lupei, T. Taira, A. Ikesue, K. Yoshida, Thermal-birefringence-induced depolarization in Nd:YAG ceramics, Opt. Lett. 27 (2002) 234–236.

[30] W. Koechner, D.K. Rice, Effect of birefringence on the performance of linearly polarized YAG:Nd lasers, IEEE J. Quantum Electron. QE-6 (1970) 556–557.

[31] I. Shoji, T. Taira, Intrinsic reduction of the depolarization loss in solid-state lasers by use of a (110)-cut Y$_3$Al$_5$O$_{12}$ crystal, Appl. Phys. Lett. 80 (2002) 3048–3050.

[32] T.Y. Fan, Heat generation in Nd:YAG and Yb:YAG, IEEE J. Quantum Electron. QE-29 (1993) 1457–1459.

[33] V. Lupei, T. Taira, A. Lupei, N. Pavel, I. Shoji, A. Ikesue, Spectroscopy and laser emission under hot band resonant pump in highly doped Nd:YAG ceramics, Opt. Commun. 195 (2001) 225–232.

[34] V. Lupei, A. Lupei, N. Pavel, T. Taira, I. Shoji, A. Ikesue, Laser emission under resonant pump in the emitting level of concentrated Nd:YAG ceramics, Appl. Phys. Lett. 79 (2001) 590–592.

[35] R. Lavi, S. Jackel, Thermally boosted pumping of neodymium lasers, Appl. Opt. 39 (2000) 3093–3098.

[36] V. Lupei, A. Lupei, S. Georgescu, T. Taira, Y. Sato, A. Ikesue, The effect of Nd concentration on the spectroscopic and emission decay properties of highly doped Nd:YAG ceramics, Phys. Rev. B 64 (2001) 092102.

[37] V. Lupei, N. Pavel, T. Taira, Basic enhancement of the overall optical efficiency of intracavity frequency-doubling devices for the one-micron continuous-wave Nd:Y$_3$ Al$_5$O$_{12}$ laser emission, Appl. Phys. Lett. 83 (2003) 3653–3655.

[38] Y. Sato, T. Taira, N. Pavel, V. Lupei, Laser operation with near quantum-defect slope efficiency in Nd:YVO$_4$ under direct pumping into the emitting level, Appl. Phys. Lett. 82 (2003) 844–846.

[39] V. Lupei, N. Pavel, Y. Sato, T. Taira, Highly efficient 1063-nm continuous-wave laser emission in Nd:GdVO$_4$, Opt. Lett. 28 (2003) 2366–2368.

[40] T.Y. Fan, Room-temperature diode-pumped Yb:YAG laser, Opt. Lett. 14 (1991) 1089–1091.

[41] T. Taira, W.M. Tulloch, R.L. Byer, Modeling of quasi-three-level lasers and operation of CW Yb:YAG lasers, Appl. Opt. 36 (1997) 1867–1874.

[42] U. Brauch, A. Giesen, M. Karszewski, Chr. Stewen, A. Voss, Multiwatt diode-pumped Yb:YAG thin disk laser continuously tunable between 1018 and 1053 nm, Opt. Lett. 20 (1995) 713–715.

[43] J. Saikawa, S. Kurimura, N. Pavel, I. Shoji, T. Taira, Performance of widely tunable Yb:YAG microchip lasers, OSA TOPS on Advanced Solid-State Lasers 34 (2000) 106–111;
J. Saikawa, S. Kurimura, I. Shoji, T. Taira, Tunable frequency-doubled Yb:YAG microchip lasers, Opt. Mat. 19 (2002) 169–174.

[44] E. Innerhofer, T. Südmeyer, F. Brunner, R. Häring, A. Aschwanden, R. Paschtta, C. Hönninger, M. Kumkar, U. Keller, 60-W average power in 810-fs pulses from a thin-disk Yb:YAG laser, Opt. Lett. 28 (2003) 367–369.

[45] C. Stewen, K. Contag, M. Larionov, A. Giesen, H. Hugel, A 1-kW CW thin disc laser, IEEE J. Selected Topics in Quantum Electron. 6 (2000) 650–657.

[46] N. Pavel, J. Saikawa, T. Taira, Radial-pumped microchip high-power composite Yb:YAG laser: design and power characteristics, Jpn. J. Appl. Phys. 40 (2001) 146–152.

[47] T. Dascalu, N. Pavel, T. Taira, 90 W continuous-wave diode edge-pumped microchip composite Yb:Y$_3$Al$_5$O$_{12}$ laser, Appl. Phys. Lett. 83 (2003) 4086–4088.

[48] M. Tsunekane, T. Taira, 300 W continuous-wave operation of diode edge-pumped, hybrid composite Yb:YAG microchip laser, Opt. Lett. 31 (2006) 2003–2005.

[49] J. Saikawa, Y. Sato, T. Taira, A. Ikesue, Passive mode locking of a mixed garnet Yb:Y$_3$ScAl$_4$O$_{12}$ ceramic laser, Appl. Phys. Lett. 85 (2004) 5845–5847.